Letter

Electrically switchable large near-infrared optical diode effect in an iron-based oxide

Asuka Ochi, Shunsuke Izumikawa, and Kenta Kimura*
Department of Materials Science, Osaka Metropolitan University, Osaka 599–8531, Japan

(Received 17 March 2025; accepted 27 May 2025; published 17 June 2025)

We report a large near-infrared (NIR) optical diode effect (ODE) and its electric field switching in the antiferromagnetic state of $LiFePO_4$. The difference in absorption coefficients for light travelling in opposite directions, divided by the sum, reaches ∼25% at a photon energy of 1.18 eV. Symmetry analysis attributes the ODE to the spin-allowed d-d transitions of octahedrally coordinated Fe^{2+} via the spin-orbit interaction. Given the abundance of iron and potentially high magnetic transition temperature in iron-based materials, this study may open the door to the application of the NIR ODE.

DOI: 10.1103/h3by-nb67

Optical absorption of materials with broken space-inversion and time-reversal symmetries, such as chiral materials subjected to an external magnetic field and linear magnetoelectric (ME) materials, can be different between light beams propagating along forward (+**k**) and backward (−**k**) directions [1–22]. This peculiar optical phenomenon is called directional dichroism or optical diode effect (ODE) [11,13,20] and has recently been used as an efficient imaging tool of antiferromagnetic domains [4,17,18,21,22]. Moreover, an ultimate ODE, that is, one-way transparency of light, potentially finds applications to novel nonreciprocal optical devices. Previous studies have observed the ODE over a wide range of wavelengths, from visible light to microwaves. For the visible and near-infrared regions, the ODE arises from either the d-d transitions of transition metal ions or the f-f transitions of rare-earth ions. A large ODE, with a relative change in the absorption coefficient (α) between +**k** and −**k** exceeding 10%, has been observed in magnetically ordered states of various 3d transition metal oxides containing Cu [8,18], Ni [19,20], and Co [21]. In particular, CuB_2O_4 exhibits one-way transparency at 1.40 eV, albeit in very high magnetic field (∼53 T) [12]. However, the magnetic transition temperatures of these Cu, Ni, and Co-based materials, and thus the onset temperatures of their ODEs, are low, well below the boiling point of nitrogen. In addition, Cu, Ni, and Co are rare elements which are unfavorable for applications. In this respect, magnetic materials based on abundant Fe elements are appealing as they often exhibit high magnetic transition temperatures. Indeed, a high temperature ODE has been observed for $GaFeO_3$ below 200 K, although the effect is only as small as 0.08% (at 1.28 eV at 4.2 K) [7]. Therefore, the development of a strategy to achieve a large ODE in Fe-based materials is crucial toward practical applications of this effect.

The $3d^5$ configuration of Fe^{3+} in $GaFeO_3$ is a half-filled high-spin state, resulting in the d-d transitions to be nominally spin forbidden. In contrast, the d-d transitions of Cu^{2+}, Ni^{2+}, and Co^{2+} ions, responsible for the above-mentioned large ODE, are spin allowed [8,18–21]. While the magnitude of the ODE is determined by multiple factors, the spin-forbidden nature of Fe^{3+} may be responsible for the small ODE. In support of this hypothesis, $MnTiO_3$, which contains Mn^{2+} with the same $3d^5$ configuration as Fe^{3+}, also exhibits a small ODE of 0.1% at 2.15 eV [16]. This consideration suggests that Fe-based materials with nontrivalent Fe ions, where d-d transitions are spin allowed, potentially exhibit large ODEs.

In this Letter, to verify the possibility of the large ODE in Fe-based materials, we have selected $LiFePO_4$, a representative Fe^{2+}-based linear ME antiferromagnetic (AFM) oxide, and measured its absorption spectra in the visible and near-infrared regions. Although the AFM transition temperature of $LiFePO_4$ ($T_N = 50$ K) is not very high, sufficient information on its magnetic, ME, and optical transitions are available, making this material suitable for the present purpose. Using this information we have discussed the origin of the ODE in terms of the spin-allowed d-d transitions of Fe^{2+} through the spin-orbit interaction (SOI).

$LiFePO_4$ with an olivine-type structure (*Pnma*) [23] is a well-known material for commercial lithium battery cathodes [24], but it has also been the focus of extensive research due to its unusual magnetism and linear ME effect [23,25–31], i.e., the linear induction of magnetization (electric polarization) with an applied electric (magnetic) field. It has been reported that an AFM transition occurs at $T_N = 50$ K [23], below which the ordered Fe^{2+} spins are predominantly oriented along the b axis with a slight overall rotation of 1.3(1)° from the b axis [26,29]. Figure 1(a) illustrates the magnetic structure in which the spin rotation is ignored. It belongs to the magnetic point group mmm' [23], breaks space-inversion and time-reversal symmetries, and allows an ODE for light propagating along the c axis (**k**∥c) [18,20–22]. Consequently, the spin rotation is not directly relevant to the emergence of the ODE and is not addressed in the present study. The mmm' symmetry also allows the linear ME effect with nonzero ME tensor components of α_{ab} and α_{ba} ($\alpha_{ab} \neq \alpha_{ba}$) [32].

Transparent yellow-green single crystals of $LiFePO_4$ were grown by the flux method [33]. The magnetization measurement of the crystal shows T_N of 50 K [34], in agreement with the previous report [23]. The α spectra for **k**∥c were measured at 40 K < T_N in the photon energy range from

*Contact author: kentakimura@omu.ac.jp

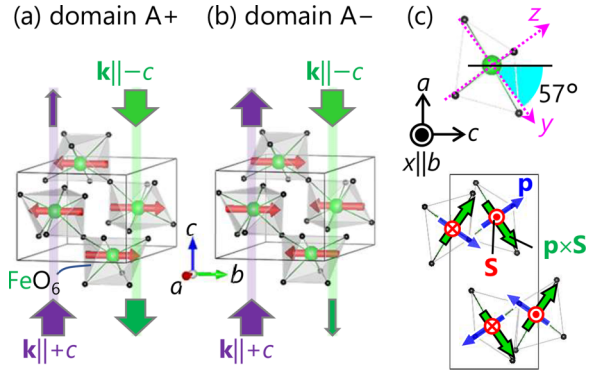

FIG. 1. (a), (b) Crystal and magnetic structures of $LiFePO_4$ for a pair of time-reversed antiferromagnetic domains A+ (a) and A− (b). A collinear antiferromagnetic structure with Fe^{2+} spins (red arrows) oriented along the b axis is assumed. For clarity, only Fe (green balls) and O atoms (black balls) are depicted. The unit cell (gray box) contains four crystallographically equivalent FeO_6 octahedra. The ODE is opposite in sign for A+ and A−, as indicated by purple and green arrows whose width denote the intensity of light. (c) A b-axis view of the crystal and magnetic structures. The FeO_6 has a pseudo-$2_z m_x m_y$ symmetry, where x, y, and z are the local coordinate axes on each FeO_6, with an angle between c and y being $\approx 57^\circ$, as shown on the top panel. The bottom panel depicts the geometrical relationship among a local electric dipole $\mathbf{p}$ along the z axis (blue arrows), the Fe^{2+} spin $\mathbf{S}$ (red crosses and dots), and a quantity $\mathbf{p} \times \mathbf{S}$ (green arrows). The $\mathbf{p} \times \mathbf{S}$ of the four FeO_6 octahedra are noncollinear with the same c-axis component.

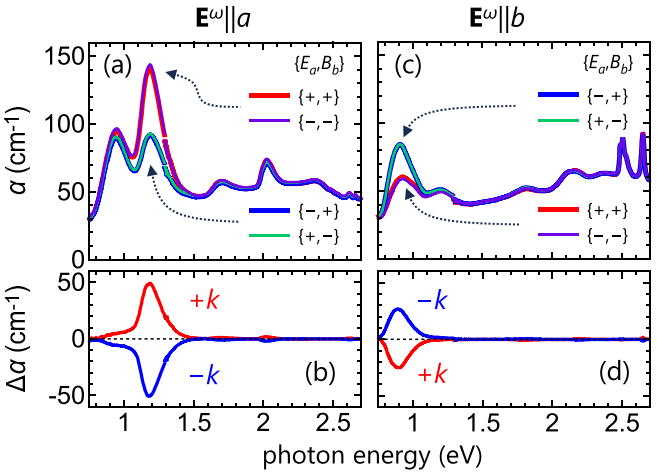

FIG. 2. Demonstration of the optical diode effect at 40 K. (a) Absorption coefficient (α) spectra for $\mathbf{E}^\omega \| a$ and $\mathbf{k} \| +c$. The red, blue, green, and purple colored data were obtained after the ME cooling with {+,+}, {−,+}, {+,−}, and {−,−}, respectively. Here, the left and right signs in parentheses denote the signs of E_a and H_b during the ME cooling, respectively, and $|E_a| = 130$ kV/m and $|H_b| = 2$ kOe. The E_a and H_b were removed before each measurement to examine a nonvolatile effect. (b) Difference α spectra between the A+ and A− domains, $\Delta\alpha = \alpha_+ - \alpha_-$, for $+k$ ($\mathbf{k} \| +c$, red curve) and $-k$ ($\mathbf{k} \| -c$, blue curve), which are obtained by subtracting the α spectrum for {−,+} from that for {+,+}. (c), (d) Spectra of α (c) and $\Delta\alpha$ (d) at for $\mathbf{E}^\omega \| b$ measured in the same way as in (a) and (b), respectively.

0.75 to 2.70 eV using a homebuilt fiber-based optical system [18,20]. The ODE is opposite in sign between a pair of time-reversed 180° AFM domains [denoted as A+ and A−, see Figs. 1(a) and 1(b)], because time reversal operation also reverses $\mathbf{k}$. Consequently, the ODE can be evaluated as the difference between α for A+ (α_+) and α for A−(α_-). To select the domain prior to the acquisition of each spectrum, the sample was cooled from 55 to 40 K (through T_N) in an electric field along the a axis (E_a) and a magnetic field along the b axis (H_b). This procedure is referred to as ME cooling. The free energy for the mmm' symmetry contains the linear ME coupling term, $\alpha_{ab} E_a H_b$ [32], where the sign of α_{ab} is opposite between A+ and A−. This allows for selecting the domain according to the sign of $E_a H_b$ during the ME cooling. Here, we define the domains selected by $E_a H_b > 0$ and $E_a H_b < 0$ as A+ and A−, respectively. After the ME cooling, both E_a and H_b are turned off to observe a spontaneous ODE. The measurements were performed for two directions of light polarization, $\mathbf{E}^\omega \| a$ and $\mathbf{E}^\omega \| b$. The details of the experiments are given in the Supplemental Material [34]. The crystal structures in Fig. 1 were drawn by using VESTA software [35].

Figure 2(a) shows the α spectra for $\mathbf{E}^\omega \| a$ and $\mathbf{k} \| +c$ measured at 40 K after four ME cooling conditions {+,+}, {−,+}, {+,−}, and {−,−}. Here, the left and right signs in the parentheses denote the signs of E_a and H_b during the ME cooling, respectively, where $|E_a| = 130$ kV/m and $|H_b| = 2$ kOe. The α spectra are approximately the same between {+,+} and {−,−} and also between {+,−} and {−,+}. However, these two sets of spectra are significantly different from each other below 1.5 eV. This means that the difference in α is not due to the difference in sign of either E_a or H_b, but to the difference in sign of $E_a H_b$ and thus the selected AFM domain (A+ or A−). By subtracting the α spectrum for {−,+} from that for {+,+}, we extract the domain dependent difference, $\Delta\alpha = \alpha_+ - \alpha_-$, which represents the ODE as mentioned above. As shown in Fig. 2(b), the $\Delta\alpha$ spectrum takes a maximum of $50\,\mathrm{cm}^{-1}$ at 1.18 eV. The magnitude of $\Delta\alpha$ does not increase with increasing $|E_a|$ and $|H_b|$, suggesting that the ME cooling achieves the monodomain state. Furthermore, the $\Delta\alpha$ spectrum is fully reversed for counterpropagating light ($\mathbf{k} \| -c$), confirming that the finite $\Delta\alpha$ is unambiguously due to the ODE. Figures 2(c) and 2(d) present a series of α and $\Delta\alpha$ spectra for $\mathbf{E}^\omega \| b$, respectively, obtained by the same measurement as for $\mathbf{E}^\omega \| a$. The finite $\Delta\alpha$ and its reversal between $\mathbf{k} \| +c$ and $\mathbf{k} \| -c$ are observed, demonstrating that the ODE also occurs for $\mathbf{E}^\omega \| b$, with the maximum magnitude reaching $\sim 20\,\mathrm{cm}^{-1}$ at 0.87 eV.

Figure 3(a) shows the temperature dependence of α_+, α_-, and $\Delta\alpha$ for $\mathbf{E}^\omega \| a$ and $\mathbf{k} \| +c$ at 1.18 eV, where $\Delta\alpha$ is the maximum. Below 50.4 K, the α_+ and α_- deviate and correspondingly the $\Delta\alpha$ becomes finite. This onset temperature is in good agreement with T_N determined by the magnetization measurement, showing that the ODE arises from the AFM order. Moreover, the temperature dependence of $\Delta\alpha$ scales linearly with that of the AFM order parameter $\langle S \rangle$ (taken from Ref. [29]). Such a scaling is also observed for $\mathbf{E}^\omega \| b$ (see the Supplemental Material [34]). These results show that the observed ODE is proportional to the ordered component of the Fe^{2+} spins.

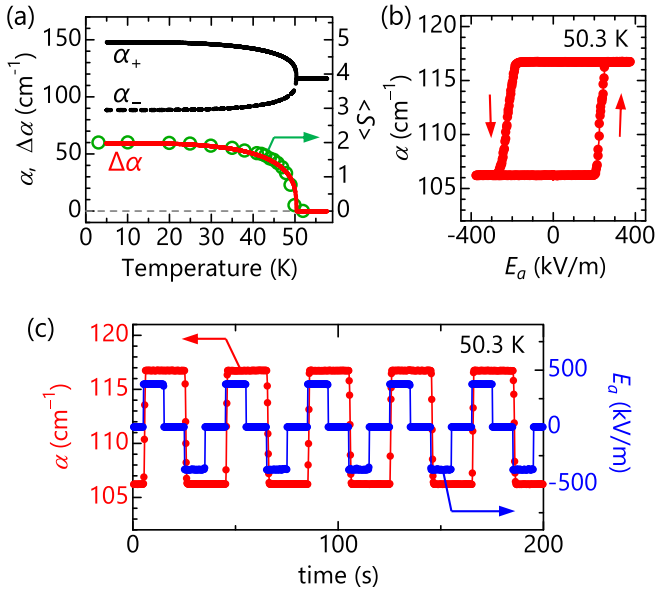

FIG. 3. Temperature dependence of the optical diode effect and its electric-field switching. All the data presented here were collected at a fixed photon energy of 1.18 eV for $\mathbf{E}^{\omega}\|a$ and $\mathbf{k}\|+c$. (a) Temperature dependence of α_+, α_-, and $\Delta\alpha = \alpha_+ - \alpha_-$. Before measuring α_+ and α_-, the ME cooling with $\{+,+\}$ and $\{-,+\}$ ($|E_a| = 130$ kV/m and $|H_b| = 2$ kOe) was applied, respectively, and then these fields were turned off. The AFM order parameter $\langle S\rangle$ (green circles) taken from Ref. [29] is plotted on the right axis. (b) E_a dependence of α and (c) temporal evolution of α responding to periodically applied E_a at $H_b = 5$ kOe and 50.3 K.

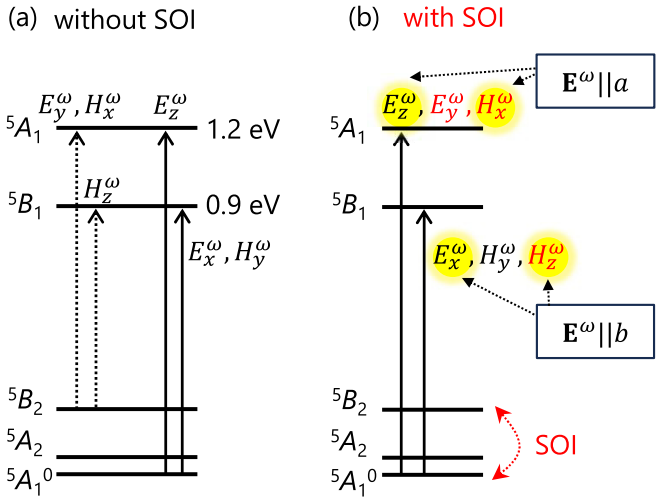

FIG. 4. Energy scheme of Fe^{2+} orbital states for C_{2v} symmetry (a) without and (b) with considering the spin orbit interaction (SOI). Orbital hybridization between $^5A_1^0$ and $^5B_2$ due to the L_xS_x term in the SOI is indicated by the curved double-headed arrow in (b). Solid vertical arrows in (a) and (b) represent possible spin-allowed d-d transitions from the ground state to $^5A_1$ and $^5B_1$, driven by E_i^{ω} (H_i^{ω})($i = x, y, z$). In (a), possible spin-allowed d-d transitions from $^5B_2$ to $^5A_1$ and $^5B_1$ are also indicated by dotted vertical arrows. In the experiment with $\mathbf{k}\|c$ and $\mathbf{E}^{\omega}\|a$ ($\mathbf{E}^{\omega}\|b$), the light contains E_z^{ω}, E_y^{ω}, and H_x^{ω} (E_x^{ω}, H_y^{ω}, and H_z^{ω}) components. The components highlighted in yellow contribute to the ODE.

To compare the magnitude of the observed ODE with those reported for other materials, we quantify the magnitude using $|\Delta\alpha/\alpha_0| \times 100\%$ defined in Ref. [20], where $\alpha_0 = \alpha_+ + \alpha_-$. With this definition, the one-way transparency corresponds to 100%. Using the data presented in Fig. 3(a) and Fig. S3 of the Supplemental Material [34], we obtain $|\Delta\alpha/\alpha_0|$ of 25% and 18% for $\mathbf{E}^{\omega}\|a$ (1.18 eV) and $\mathbf{E}^{\omega}\|b$ (0.89 eV), respectively, at 5 K. These values are comparable to those for Cu [8,18], Ni [19,20], and Co [21] based materials and more than two orders of magnitude greater than those for $GaFeO_3$ [7] and $MnTiO_3$ [16].

Furthermore, we investigate an isothermal response of the ODE to an applied electric field. Since the ME free energy ($\alpha_{ab}E_aH_b$) is opposite in sign between A+ and A−, the application of a sufficiently strong E_a in the presence of a bias H_b can switch the AFM domains, resulting in the switching of the ODE. Figure 3(b) shows the E_a dependence of α at 1.18 eV for $\mathbf{E}^{\omega}\|a$ in $H_b = 5$ kOe, measured at 50.3 K just below T_N. The α changes abruptly at about +230 and −220 kV/m for E_a-up and E_a-down sweepings, respectively, demonstrating the hysteretic switching of the ODE. As shown in Fig. 3(c), both the larger and smaller α values at $E_a = 0$ remain constant for a periodically applied E_a, indicating that the ODE in $LiFePO_4$ is robust against the electric field switching.

The microscopic mechanism of the ODE in the visible and near-infrared regions is generally due to an interference between electric dipole (E1) and magnetic dipole (M1) transitions through SOI [2,7,8,12,15–20], and such transitions are dominated by the on-site d-d transitions for $3d$ transition metal oxides. As shown in Fig. 1(a), there are four crystallographically equivalent Fe^{2+} ions [labeled as Fe(l) with $l = 1$–4] in the unit cell of $LiFePO_4$. A contribution to the ODE from each Fe(l), $\Delta\alpha^l$, can be expressed as [12,18,20]

$$\begin{aligned}\Delta\alpha^l = \alpha_{+k}^l - \alpha_{-k}^l &\propto |\langle e|H_{\mathrm{E1}}|g\rangle + \langle e|H_{\mathrm{M1}}|g\rangle|^2 \\ &- |\langle e|H_{\mathrm{E1}}|g\rangle - \langle e|H_{\mathrm{M1}}|g\rangle|^2 \\ &= 4\mathrm{Re}[\langle g|H_{\mathrm{E1}}|e\rangle\langle e|H_{\mathrm{M1}}|g\rangle]. \end{aligned} \quad (1)$$

Here, H_{E1} (H_{M1}) is the E1 transition operator related to an electric (magnetic) component of light and g (e) denotes the ground (excited) state wavefunction of each Fe(l). As shown in Fig. 1(c), Fe^{2+} in $LiFePO_4$ occupies the $4c$ Wyckoff position and is coordinated by a noncentrosymmetric oxygen octahedron, with symmetry C_v (m_x) but close to C_{2v} ($2_z m_x m_y$) [36], where x, y, and z are the local coordinate axes defined such that z is along the twofold axis, x is parallel to the b axis to which the ordered Fe^{2+} spins ($\mathbf{S}$) are oriented, and y is orthogonal to both x and z. In the $2_z m_x m_y$ symmetry, each FeO_6 octahedron has a local electric dipole $\mathbf{p}$ along the z axis [Fig. 1(c)]. As discussed in Ref. [20], the combination of $\mathbf{p}$ and $\mathbf{S}$ of each FeO_6 can lead to a local ODE for $\mathbf{k}\|(\mathbf{p}\times\mathbf{S})\|y$. Although $\mathbf{p}\times\mathbf{S}$ of the four FeO_6 octahedra are mutually canted, the c-axis component is the same, so the overall ODE (i.e., observed $\Delta\alpha$) for $\mathbf{k}\|c$ should be the sum of $\Delta\alpha^l$ for $\mathbf{k}\|c$ over $l = 1$–4. Therefore, considering the optical transition processes on a single FeO_6 octahedron is sufficient to discuss the origin of the observed ODE.

Figure 4(a) illustrates the energy levels of Fe^{2+} $3d$ orbital states within the C_{2v} approximation for $LiFePO_4$ in the absence of SOI, which are based on those previously reported for the isostructural $LiFe_{1-x}Mn_xPO_4$ [37,38] and Fe_2SiO_4 [36,39]. The C_{2v} crystal field splits the ^{5}D multiplet for free Fe^{2+} into five nondegenerate levels: the ground state $^5A_1$ (hereafter denoted as $^5A_1^0$ to distinguish it from the excited state $^5A_1$), slightly higher energy excited states $^5A_2$ and $^5B_2$, and well separated excited states $^5B_1$ and $^5A_1$. The energy levels of these states are ordered from lowest to highest as follows: $^5A_1^0$, $^5A_2$, $^5B_2$, $^5B_1$, and $^5A_1$. The group theory indicates that $^5A_1^0 \rightarrow {}^5B_1$ is E1 allowed by E_x^ω, and M1 allowed by H_y^ω, while $^5A_1^0 \rightarrow {}^5A_1$ is E1 allowed by E_z^ω, where E_i^ω $(H_i^\omega)(i = x, y, z)$ is an oscillating electric (magnetic) field of light along the i axis. Based on this energy scheme, the broad peaks associated with the large ODE at ∼0.9 and ∼1.2 eV [Figs. 2(a) and 2(c)] are assigned to the spin-allowed d-d transitions $^5A_1^0 \rightarrow {}^5B_1$ and $^5A_1$, respectively. In contrast, the sharp peaks observed at 2.5 ∼ 2.7 eV for $\mathbf{E}^\omega \| b$ [Fig. 2(c)] are probably due to spin-forbidden d-d transitions [37], leading to only a weak ODE [Fig. 2(d)]. To explain the large ODE at 0.9 and 1.2 eV, the SOI must be considered because $\langle g|H_{E1}|e\rangle\langle e|H_{M1}|g\rangle$ in Eq. (1) in the absence of SOI is imaginary, and thus $\Delta\alpha^l$ becomes zero [15]. As the ordered Fe^{2+} spins are oriented along the x axis (S_x), we consider an L_xS_x term in the SOI, where L_x denotes the orbital angular momentum along the x axis. Because L_x belongs to B_1 symmetry, the L_xS_x term hybridizes the orbital states $^5A_1$ ($^5A_1^0$) and $^5B_2$, as well as $^5B_1$ and $^5A_2$. Of these hybridizations, we focus only on the hybridization between $^5A_1^0$ and $^5B_2$ as the expected energy difference between $^5A_1^0$ and $^5B_2$ (∼0.2 eV [36,37] or ∼0.3 eV [38]) is closest to the typical strength of SOI for Fe^{2+} (∼0.05 eV [40]), making the hybridization significant. The resulting inclusion of the $^5B_2$ component in the ground state allows for additional transitions from the ground state to $^5B_1$ by H_z^ω and to $^5A_1$ by E_y^ω and H_x^ω [Fig. 4(b)]. These SOI-mediated E1 or M1 transitions can induce the ODE when they interfere with the originally allowed M1 or E1 transitions. In the present experiment with $\mathbf{k} \| c$, the $\mathbf{E}^\omega \| a$ $(\mathbf{E}^\omega \| b)$ polarized light possesses the E_z^ω, E_y^ω, and H_x^ω (E_x^ω, H_y^ω, and H_z^ω) components [see Fig. 1(c)]. Consequently, the ODE can occur at ∼1.1 eV for $\mathbf{E}^\omega \| a$ (∼0.9 eV for $\mathbf{E}^\omega \| b$) due to the interference between the E_z^ω- (E_x^ω-)driven E1 transition and the SOI-mediated, H_x^ω- (H_z^ω-)driven M1 transition to the $^5A_1$ ($^5B_1$) state, consistent with the observations [Figs. 2(c) and 2(d)]. Therefore, the observed ODE is well explained by spin-allowed Fe^{2+} d-d transitions assuming the C_{2v} symmetry and the b-axis collinear AFM structure.

The local ODE is maximal for $\mathbf{k} \| (\mathbf{p} \times \mathbf{S}) \| y$, because under this condition there are no E_y^ω and H_y^ω components that are irrelevant to this effect. However, it is impossible to satisfy this condition simultaneously for the four FeO_6 octahedra due to the mutual canting of $\mathbf{p}$ and thus $\mathbf{p} \times \mathbf{S}$ [Fig. 1(c)]. This reduces the overall ODE by a factor of $\cos 57^\circ \approx 0.54$. Therefore, optimizing the orientation of the FeO_6 octahedra, and thus $\mathbf{p}$, can further enhance the overall ODE.

In conclusion, we have observed a large, electrically switchable optical diode effect (ODE) at near-infrared wavelengths in the Fe^{2+}-based magnetoelectric antiferromagnet $LiFePO_4$. The observed optical diode effect is adequately explained by the spin-allowed d-d transitions of octahedrally coordinated Fe^{2+} through the spin-orbit interaction. Other Fe^{2+}-based magnetic materials can also exhibit a comparable or even more pronounced ODE in the similar wavelength range, if they have octahedrally coordinated Fe^{2+} and belong to the magnetic point group that allows the ODE. Candidates listed in MAGNDATA [41] include $FeSb_2O_4$ [42,43], $Fe_3(PO_4)_2$ [44], and $Fe_4Nb_2O_9$ [45]. Given the abundance of Fe and the possibility of high magnetic transition temperature in Fe-based materials, this study may pave the way for developing electrically controllable nonreciprocal optical devices.

K.K. acknowledges support from JSPS KAKENHI Grants No. JP23K17663 and No. JP24K00575 and the Iketani Science and Technology Foundation.

The data that support the findings of this article are openly available [46].

[1] L. D. Barron and J. Vrbancich, Mol. Phys. **51**, 715 (1984).
[2] T. Arima, J. Phys.: Condens. Matter **20**, 434211 (2008).
[3] D. Szaller, S. Bordács, and I. Kézsmárki, Phys. Rev. B **87**, 014421 (2013).
[4] K. Kimura and T. Kimura, APL Mater. **11**, 100902 (2023).
[5] G. L. J. A. Rikken and E. Raupach, Nature (London) **390**, 493 (1997).
[6] G. L. J. A. Rikken, C. Strohm, and P. Wyder, Phys. Rev. Lett. **89**, 133005 (2002).
[7] J. H. Jung, M. Matsubara, T. Arima, J. P. He, Y. Kaneko, and Y. Tokura, Phys. Rev. Lett. **93**, 037403 (2004).
[8] M. Saito, K. Taniguchi, and T. Arima, J. Phys. Soc. Jpn. **77**, 013705 (2008).
[9] Y. Shimada, H. Kiyama, and Y. Tokura, J. Phys. Soc. Jpn. **77**, 033706 (2008).
[10] I. Kézsmárki, D. Szaller, S. Bordács, V. Kocsis, Y. Tokunaga, Y. Taguchi, H. Murakawa, Y. Tokura, H. Engelkamp, T. Rõõm, and U. Nagel, Nat. Commun. **5**, 3203 (2014).
[11] I. Kézsmárki, U. Nagel, S. Bordács, R. S. Fishman, J. H. Lee, H. T. Yi, S.-W. Cheong, and T. Rõõm, Phys. Rev. Lett. **115**, 127203 (2015).
[12] S. Toyoda, N. Abe, S. Kimura, Y. H. Matsuda, T. Nomura, A. Ikeda, S. Takeyama, and T. Arima, Phys. Rev. Lett. **115**, 267207 (2015).
[13] S. Yu, B. Gao, J. W. Kim, S.-W. Cheong, M. K. L. Man, J. Madéo, K. M. Dani, and D. Talbayev, Phys. Rev. Lett. **120**, 037601 (2018).
[14] V. Kocsis, K. Penc, T. Rõõm, U. Nagel, J. Vít, J. Romhányi, Y. Tokunaga, Y. Taguchi, Y. Tokura, I. Kézsmárki, and S. Bordács, Phys. Rev. Lett. **121**, 057601 (2018).
[15] M. O. Yokosuk, H.-S. Kim, K. D. Hughey, J. Kim, A. V. Stier, K. R. O'Neal, J. Yang, S. A. Crooker, K. Haule, S.-W. Cheong, D. Vanderbilt, and J. L. Musfeldt, npj Quantum Mater. **5**, 20 (2020).
[16] T. Sato, N. Abe, S. Kimura, Y. Tokunaga, and T. Arima, Phys. Rev. Lett. **124**, 217402 (2020).

[17] K. Kimura, T. Katsuyoshi, Y. Sawada, S. Kimura, and T. Kimura, Commun. Mater. **1**, 39 (2020).
[18] K. Kimura, Y. Otake, and T. Kimura, Nat. Commun. **13**, 697 (2022).
[19] K. Park, M. O. Yokosuk, M. Goryca, J. J. Yang, S. A. Crooker, S.-W. Cheong, K. Haule, D. Vanderbilt, H.-S. Kim, and J. L. Musfeldt, npj Quantum Mater. **7**, 38 (2022).
[20] K. Kimura and T. Kimura, Phys. Rev. Lett. **132**, 036901 (2024).
[21] B. Tóth, V. Kocsis, Y. Tokunaga, Y. Taguchi, Y. Tokura, and S. Bordács, Phys. Rev. B **110**, L100405 (2024).
[22] M. Moromizato, T. Miyake, T. Masuda, T. Kimura, and K. Kimura, Phys. Rev. Lett. **133**, 086701 (2024).
[23] R. P. Santoro and R. E. Newnham, Acta Crystallogr. **22**, 344 (1967).
[24] M. Dubarry and B. Y. Liaw, J. Power Sources **194**, 541 (2009).
[25] M. Mercier, P. Bauer, and B. Fouilleux, C. R. Acad. Sc. Paris **267**, 1345 (1968).
[26] J. Li, V. O. Garlea, J. L. Zarestky, and D. Vaknin, Phys. Rev. B **73**, 024410 (2006).
[27] G. Liang, K. Park, J. Li, R. E. Benson, D. Vaknin, J. T. Markert, and M. C. Croft, Phys. Rev. B **77**, 064414 (2008).
[28] P. J. Baker, I. Franke, F. L. Pratt, T. Lancaster, D. Prabhakaran, W. Hayes, and S. J. Blundell, Phys. Rev. B **84**, 174403 (2011).
[29] R. Toft-Petersen, M. Reehuis, T. B. S. Jensen, N. H. Andersen, J. Li, M. D. Le, M. Laver, C. Niedermayer, B. Klemke, K. Lefmann, and D. Vaknin, Phys. Rev. B **92**, 024404 (2015).
[30] E. Fogh, B. Klemke, A. Pages, J. Li, D. Vaknin, H. M. Rønnow, N. B. Christensen, and R. Toft-Petersen, Physica B: Condens. Matter **648**, 414380 (2023).
[31] S. Holm-Janas, M. Akaki, E. Fogh, T. Kihara, M. D. Le, P. C. Forino, S. E. Nikitin, T. Fennell, A. Painganoor, D. Vaknin, M. Watanabe, N. B. Christensen, H. Nojiri, and R. Toft-Petersen, Phys. Rev. B **109**, 174413 (2024).
[32] J.-P. Rivera, Eur. Phys. J. B **71**, 299 (2009).
[33] V. I. Fomin, V. P. Gnezdilov, V. S. Kurnosov, A. V. Peschanskii, A. V. Yeremenko, H. Schmid, J.-P. Rivera, and S. Gentil, Low Temp. Phys. **28**, 203 (2002).
[34] See Supplemental Material at http://link.aps.org/supplemental/10.1103/h3by-nb67 for experimental details and additional experimental data (n.d.).
[35] K. Momma and F. Izumi, J. Appl. Crystallogr. **44**, 1272 (2011).
[36] W. A. Runciman, D. Sengupta, and J. T. Gourley, Am. Mineral. **58**, 451 (1973).
[37] K. Langer, M. N. Taran, and A.-M. Fransolet, Eur. J. Mineral. **18**, 337 (2006).
[38] A. Van Alboom, E. De Grave, and M. Wohlfahrt-Mehrens, Am. Mineral. **96**, 408 (2011).
[39] K. Ullrich, K. Langer, and K. D. Becker, Phys. Chem. Miner. **29**, 409 (2002).
[40] G. M. Cole and B. B. Garrett, Inorg. Chem. **9**, 1898 (1970).
[41] S. V. Gallego, J. M. Perez-Mato, L. Elcoro, E. S. Tasci, R. M. Hanson, K. Momma, M. I. Aroyo, and G. Madariaga, J. Appl. Crystallogr. **49**, 1750 (2016).
[42] J. A. Gonzalo, D. E. Cox, and G. Shirane, Phys. Rev. **147**, 415 (1966).
[43] A. Iyama, Y. Wakabayashi, N. Hanasaki, and T. Kimura, Jpn. J. Appl. Phys. **53**, 05FB02 (2014).
[44] J. K. Warner, A. K. Cheetham, A. G. Nord, R. B. Von Dreele, and M. Yethiraj, J. Mater. Chem. **2**, 191 (1992).
[45] R. Jana, D. Sheptyakov, X. Ma, J. A. Alonso, M. Pi, A. Muñoz, Z. Liu, L. Zhao, N. Su, S. Jin, X. Ma, K. Sun, D. Chen, S. Dong, Y. Chai, S. Li, and J. Cheng, Phys. Rev. B **100**, 094109 (2019).
[46] K. Kimura, Optical and magnetization data of $LiFePO_4$ (2025), http://hdl.handle.net/10466/0002003167.